sustainability

MDPI

Article

Probing Fault Features of Lithium-Ion Battery Modules under Mechanical Deformation Loading

Anwei Zhang [1], You Zhou [1], Chengyun Wang [1,*], Shoutong Liu [2], Peifeng Huang [2,*], Hao Yan [1] and Zhonghao Bai [2]

[1] GAC Automotive Research & Development Center, Guangzhou 511434, China; zhanganwei@gacrnd.com (A.Z.); zhouyou@gacrnd.com (Y.Z.)
[2] State Key Laboratory of Advanced Design and Manufacturing Technology for Vehicle, Hunan University, Changsha 410012, China
* Correspondence: wangchengyun@gacrnd.com (C.W.); pfhuang@hnu.edu.cn (P.H.)

Abstract: Electric vehicle battery systems are easily deformed following bottom or side pillar collisions. There is a knowledge gap regarding the fault features of minor mechanical deformation without ISC, which can be used for early warning of mechanical deformation. In this study, the fault features of a lithium-ion battery module under different degrees of mechanical deformation were studied from the perspective of voltage consistency. The results show that the capacity of the battery module declines with an increase in indentation depth, consistent with the capacity degradation of the indented cell. During the charging and discharging processes, the voltage of the indented cell deviates to a lower value compared to the other normal cells. At the end of the discharging process, the voltage sharply declines and exhibits a significant deviation from the other normal cells. The Mean Normalization (MN) method is employed to quantitatively describe the voltage consistency. The results indicate that the MN value of the indented cell's voltage is distributed at the lowest during the charging period and sharply declines below −0.06 at the end of discharging. In the future, a fault detection method for mechanical abuse will be established based on these features.

Keywords: battery system; mechanical abuse; voltage consistency; mean normalization; risk management

Citation: Zhang, A.; Zhou, Y.; Wang, C.; Liu, S.; Huang, P.; Yan, H.; Bai, Z. Probing Fault Features of Lithium-Ion Battery Modules under Mechanical Deformation Loading. *Sustainability* **2023**, *15*, 11928. https://doi.org/10.3390/su151511928

Academic Editor: Noradin Ghadimi

Received: 8 May 2023
Revised: 27 July 2023
Accepted: 28 July 2023
Published: 3 August 2023

1. Introduction

To mitigate problems arising from global warming, environmental pollution, and depletion of fossil fuels, electric vehicles (EVs) have been widely adopted and developed worldwide. Recently, lithium-ion batteries (LIBs) have become the main energy source for EVs due to their advantages of long cycle life, high energy density, and zero emissions. However, the low thermal stability of active materials in LIBs makes them prone to failure, including thermal runaway, when subjected to abusive conditions [1]. As the number of EVs on the road increases, there has been growing concern about battery-related accidents caused by battery failures [2].

These abusive conditions can be categorized into three types: mechanical, electrical, and thermal [3,4]. Mechanical abuse includes penetration, compression, and crashes [5]; thermal abuse includes exposure to high external temperatures and fire impingement [1]; electrical abuse involves external short circuits, overcharging, over-discharging, etc. [4,6,7]. However, these three types of abuse often occur in combination, interacting with and promoting each other. For example, in most situations, mechanical abuse leads to electrical abuse, and the electrical abuse is often accompanied by heat generation, which can even potentially trigger thermal abuse. Penetration and severe deformation can cause internal short circuits (ISC) within the battery. The ISC generates a large amount of heat at the point of short circuit, resulting in a localized temperature increase known as a hot spot. Electrical abuse accelerates the development of thermal abuse, eventually leading to thermal runaway [8].

To prevent battery failures caused by these abusive conditions, timely fault diagnosis and prognosis are essential for ensuring the safe operation of EVs [8,9]. These approaches can be classified into three categories: threshold-based, model-based, and data-driven methods [10]. Zhu et al. [11] employed a threshold-based method to diagnose overcharge faults by detecting whether the voltage, temperature, and rate of voltage change exceed predefined thresholds. Xiong et al. [7] proposed a model-based method to detect external short circuits by comparing the measured voltage with the predicted value using an equivalent circuit model. Wang et al. [12,13] proposed data-driven methods that utilize sample entropy, Shannon entropy, and Z-score to monitor the health status of batteries. While many methods have been proposed for fault diagnosis, most of them rely on abnormal variations in external parameters such as voltage and temperature. Among the three categories of abusive conditions, thermal and electrical abuses exhibit clear voltage and temperature signals, which can be easily used for fault diagnosis through the aforementioned methods. In situations involving mechanical abuse, a sharp drop in cell voltage and a rapid increase in local temperature occur when the cell experiences deformation-induced ISC [14,15]. However, when the deformation is minor, the resistance of the internal short circuit may be too high to cause significant voltage deviation. Qiao et al. [16] proposed a quantitative diagnosis method for ISC using the incremental capacity method, which measures the excess power consumption during the charging and discharging processes. When the deformation is too small to trigger ISC, it can be challenging to monitor the fault diagnosis signals. However, the potential risks associated with minor mechanical deformation should not be overlooked. For instance, the explosion of Samsung cell phones in 2016 was a typical incident caused by compression at the corner of the battery [17]. In April 2019, an NIO ES8 caught fire at a service outlet. The investigation revealed that the accident was caused by significant mechanical deformation of the battery pack and cooling plate resulting from a previous impact two days earlier [18]. The delayed occurrence of accidents due to mechanical deformation poses potential safety hazards, emphasizing the need to study the fault characteristics of batteries under mechanical deformation for early fault detection.

The failure mechanism of mechanical abuse has been extensively investigated. Under severe conditions, mechanical deformation can cause electrolyte leakage from the release valve and result in structural failure of the battery [19,20]. The high tensile stress experienced at fold areas can induce ISC [21,22]. Wang et al. [23] disassembled compressed cells and observed the internal structure variations using an optical microscope. They found that deformed electrodes can penetrate the separator, creating direct contact between the cathode and anode electrodes, leading to ISC and even thermal runaway. Based on different contact patterns, Santhanagopalan et al. [24] categorized ISC into four types: (1) connection between active materials at the cathode electrode and the current collector at the anode electrode; (2) connection between active materials at the cathode and anode electrodes; (3) connection between the current collectors at the cathode and anode electrodes; and (4) connection between active materials at the anode electrode and the current collector at the cathode electrode. Among these types, the highest risk is associated with active materials at the cathode electrode connecting with the current collector at the anode electrode. Factors such as state of charge (SOC), depth, and width of penetration also influence the risk level [14,15,25]. In situations involving minor deformation, ISC may disappear shortly after its occurrence due to passivation of positive and negative electrode materials or isolation of positive and negative electrodes caused by separator melting. This type of ISC is referred to as "soft ISC" [26]. The corresponding battery voltage briefly declines and then recovers to its previous value. In cases of slight mechanical deformation without ISC, researchers have found that increased restraint stress in the compression area can lead to internal damage, including loss of lithium inventory and active material, resulting in decreased cycle performance [27–29]. The copper current collector in the compressed area may break in a "mud" shape or fracture directly, and an interface layer may form on the surface of the copper foil, leading to copper foil corrosion in the interface area and increased battery impedance [30]. Slight mechanical deformation can also cause ca-

pacity loss in lithium batteries, although larger-capacity batteries are more resistant to deformation effects and experience smaller changes in capacity. The capacity change in batteries after indentation is primarily due to the loss of recoverable lithium, which is related to fragmentation of the current collector, crushing of negative active particles, and compaction of positive active materials [27]. Cyclic tests on batteries after slight indentation have shown that the rate of capacity attenuation in the indented battery is similar to that of a normal battery in the early stage of the cycle [31]. However, accelerated capacity attenuation occurs in the late stage of the cycle, mainly due to the loss of active materials and recoverable lithium [28]. Huang et al. [32] found that slight mechanical deformation can improve the cycle performance of tested cells, but the effect becomes negative as the deformation becomes more severe. These changes can be reflected in the voltage curve, and by extracting and analyzing these characteristics, it becomes possible to provide early warning for mechanical deformation.

The aforementioned research has extensively explored the damage mechanisms and corresponding fault features of mechanical deformation, ranging from severe deformation to minor deformation. However, there is a knowledge gap regarding the fault features of minor mechanical deformation without ISC for fault detection. In this study, we investigate the fault features of batteries with slight mechanical deformation from the perspective of voltage consistency. We conducted experiments on locally mechanically deformed cells and connected them in series with normal cells for cycling tests aimed at detecting fault features in voltage consistency. The Mean Normalization (MN) method was employed to analysis the changes in voltage consistency.

2. Methodology

According to a previous study [32], the capacity of the indented cell could vary with the degree of deformation. The variation in cell capacity leads to inconsistency in the capacities between cells, which is reflected in the voltages of the cells. Therefore, in this work, the consistency of the cells' voltages is used to analyze the fault feature of mechanical deformation. Before the indentation, six normal cells were connected in series and cycled five times. Then, one of these cells was taken out for indentation. The indented cell was continuously connected with the other five cells in series and cycled to study the influence of mechanical deformation on the capacity and voltage consistency of the battery module. The charge and discharge capacity and voltage curves before and after the mechanical deformation test were recorded to analyze the fault feature.

However, monitoring the deviation of voltage is difficult in real applications due to its susceptibility to noise interference. To quantitatively analyze the deviation of each cell in the battery module, the MN method is employed in this study. The *MN* value of cell voltage at t_i moment is expressed as follows:

$$MN_k^i = \frac{U_k(t_i) - \overline{U}(t_i)}{U_{max}(t_i)} \tag{1}$$

where $\overline{U}$ is the mean value of the cells' voltage in the battery module, U_{max} is the maximum cell voltage, t_i is a specific moment in the voltage curve, and k is the number of cells. In this equation, $U_i - \overline{U}$ means the deviation of each cell's voltage to the mean voltage of all cells. The MN value can be positive or negative. An increase in the absolute value of *MN* indicates a larger deviation of the cell voltage from the mean value. Unlike other error analysis methods such as root-mean-square error and mean square error, the *MN* value can reflect whether the estimated value is higher or lower than the mean value through the sign of the value and the degree of deviation. When the cells in the battery module operate normally, the *MN* value will stabilize around 0. However, if one cell experiences abusive behavior, the *MN* value could sharply increase or decrease. This method can effectively amplify the deviation feature for fault diagnosis. In addition, the *MN* method has the advantage of less computing, which can be easily used for real-time monitoring of the voltage inconsistency.

3. Experimental Tests

In this study, 18,650 commercial ternary/graphite lithium-ion battery cells (DMEGC, INR18650-26E, Donghua, China) were used. The operating voltage ranges from 2.75 V to 4.2 V. The nominal capacity of all cells is 2600 mAh. The internal resistance is less than 25 mΩ. The standard charge and discharge currents are 0.5 and 1 charge rates (C-rate), respectively. The indentation tests were conducted using an electron universal testing machine (Instron, 5980, Boston, MA, USA) as shown in Figure 1. The indenter is a semi-sphere with a diameter of 12.7 mm. To ensure safety during compression, the SOC of the tested cells was discharged to 0% before indentation. The voltages of the cells and force–displacement curve during compression were recorded to estimate ISC. The cell being tested experiences ISC when the indentation depth exceeds 7 mm, so the displacements of indentation were set at 5, 6, and 7 mm to obtain the fault features of mechanical deformation before the cell experiences ISC.

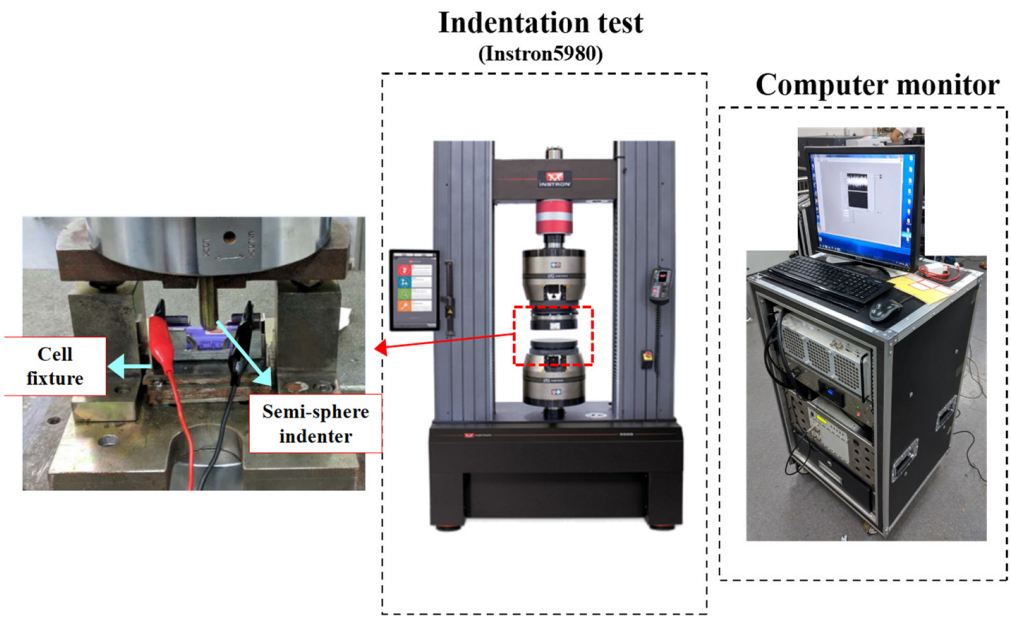

Figure 1. Electron universal testing machine for indentation tests.

To investigate the fault features of the indented cell in the battery module, cycling tests of the battery module were conducted. The experimental setup is shown in Figure 2. To obtain the features of mechanical deformation from the perspective of consistency, five normal cells and one specified cell for indentation test were connected in series and cycled by a cycle meter (Neware, CT-4002-30V60A-NA, Shengzhen, China) at room temperature. During cycling, the cells were protected by a battery management system (BMS) protector (Jikong company, JK-B1A24S15P, Chengdu, China) to prevent overcharging or over-discharging. This BMS system only enables the protection function, and the voltage of each cell in the battery module can be monitored by this system. The series-connected battery module was cycled between 17.4 V and 24.6 V. The setting of the cut-off voltages of the battery module is to limit the voltage of cells between 2.9 V and 4.1 V during charging and discharging periods. To prevent the overcharge and over-discharge of cells, 2.9 V and 4.1 V are set as the lower and upper protection voltages of cells, respectively. These limitations are that cells were charged and discharged at 1 C-rate (2.6 A) with 30 min of rest between charge and discharge periods during cycling.

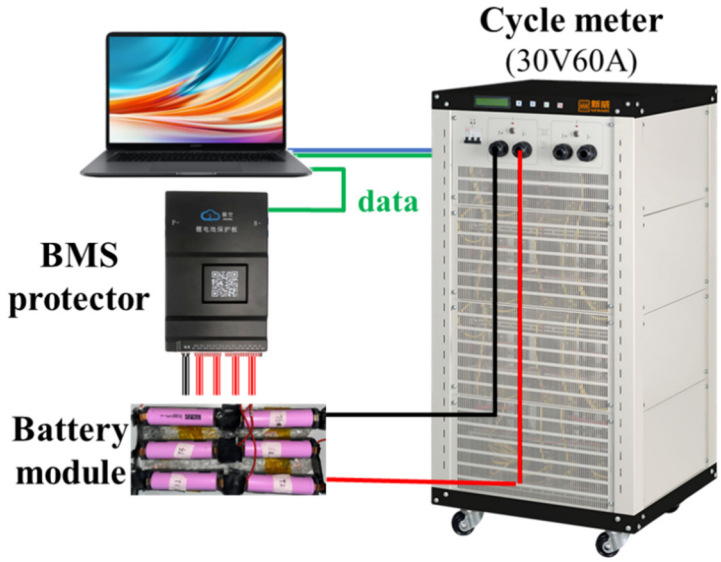

Figure 2. Experimental setup for battery module cycle test.

4. Results and Discussion

Three cells were indented at the center of the side face with depths of displacement of 5 mm, 6 mm, and 7 mm, as shown in Figure 3. The force−displacement curves during the indentation process are illustrated in the figure. The mechanical responses of the tested cells during indentation are relatively consistent, but the difference between cells enlarges with increasing depth of indentation. It can be observed that the force−displacement curves grow exponentially. As the indentation depth increases, the deformation of the battery initially starts from the battery casing and progresses to the deformation of electrode materials near the edges. Consequently, more electrode materials become involved in the mechanical deformation process, resulting in exponential stress increase with increasing displacement of indentation. The stress values reach 2239.5 N, 3876.9 N, and 6852.7 N at displacements of 5 mm, 6 mm, and 7 mm, respectively. These values are much lower than the results reported by Liu et al. [33] and Xing et al. [34]. This difference could be attributed to the variance in mechanical deformation between cylindrical cells and prismatic cells. The cylindrical cell allows for more space for deformation, making the force−displacement curve flatter compared to that of the prismatic cell.

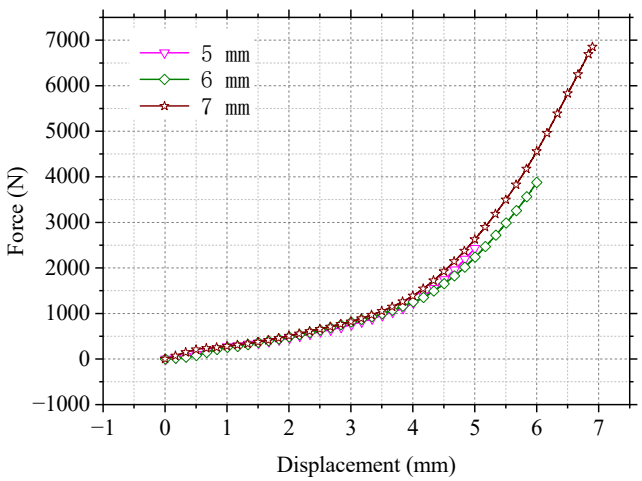

Figure 3. Force−displacement curves of tested cells during the indentation tests.

The indented cell was continuously connected with the other five cells in series and cycled five times. Figure 4 presents the variation in battery module capacity before and

after the indentation during the charging and discharging process. Figure 4a shows that the charging capacity of the battery module is approximately 2450 mAh before the indentation test. Due to energy consumption by the BMS protector and heat generation of the batteries, the discharging capacity decreases by approximately 200 mAh. When one cell in the battery module was indented by 5 mm, it can be observed that the charge and discharge capacities decrease by 18 mAh and 27 mAh, respectively. With an increase in the indentation depth to 6 mm, the average capacity of the battery module decreases by 64 mAh during the charging period and 65 mAh during the discharging period, as shown in Figure 4b. Figure 4c illustrates that the decline in the average battery module capacity increases to 132 mAh and 143 mAh during the charging and discharging process, respectively, when the indentation depth reaches 7 mm. In our previous research [32], we found that slight mechanical deformation can elevate the battery capacity, but this effect becomes negative for the cells when mechanical deformation accumulates. The capacity of the battery module is determined by the minimum cell capacity. While an increase in cell capacity might have a limited impact on the capacity of the battery module, a decline can be directly reflected by the variation in battery module capacity. Therefore, the decline in module capacity shown in Figure 4b,c could be attributed to the capacity degradation of the indented cell.

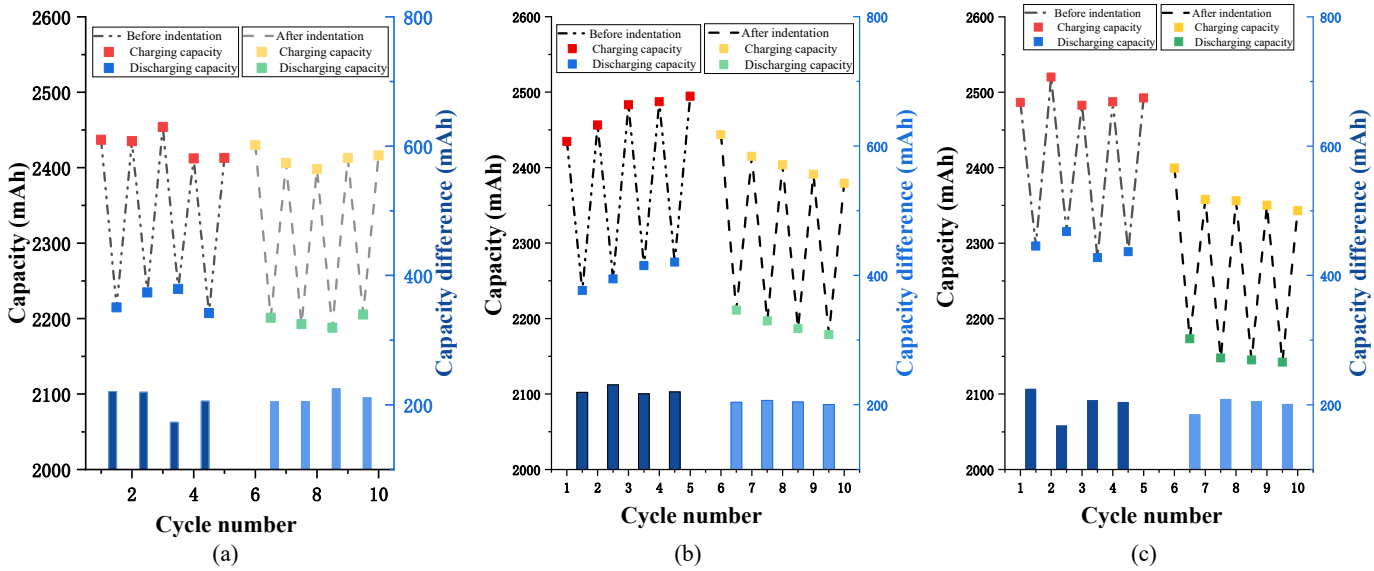

Figure 4. The variation in battery module charge capacity and discharge capacity before and after the indentation test (**a**) at 5 mm indentation depth; (**b**) at 6 mm indentation depth; (**c**) at 7 mm indentation depth.

Changes in the internal properties of batteries, such as internal resistance, health, and capacity, can directly influence voltage performance. Figure 5a shows the variation in voltage consistency caused by mechanical deformation at a 5 mm depth of indentation. Prior to subjecting the cells to mechanical abuse, the voltage of all cells should be consistent. However, due to the specified cells used for the indentation test having a higher capacity than other cells, there is an intrinsic capacity inconsistency between the specified cell and the normal cells, resulting in its voltage being higher than the other five normal cells at the end of the discharging and resting periods. This is because the same energy was discharged from these cells in the same discharge time, and the specified cell with higher capacity would have higher SOC and show higher voltage than other cells. Despite this, it can be observed that the voltage of the indented cell declines to the lowest value during the charging period compared to the voltage data of the battery module before cell deformation. At the end of the discharge process, the voltage of the indented cell sharply decreases and deviates significantly from the other normal cells. The same phenomenon can also be observed in the cycle test of the battery module after loading the mechanical abuse at

depths of indentation of 6 mm and 7 mm, as shown in Figure 5b,c. With an increase in indentation depth, the deviation becomes more pronounced. This is mainly due to the indentation causing a decrease in battery capacity. The decrease in capacity changes the characteristics of the battery from exhibiting a higher voltage at the end of discharge (typical for batteries with initially larger capacity) to exhibiting a lower voltage than the other cells. The reason is similar to the explanation for higher voltage of the specified cell at the end of the discharging period, that the indented cell with lower capacity has lower SOC and shows lower voltage than other cells after the discharge. According to our previous study [32], degraded capacity is positively correlated with the degree of mechanical deformation. Therefore, the variation of the indented cell with a 7 mm depth of displacement is greater than that of the indented cell with a 5 mm depth of displacement.

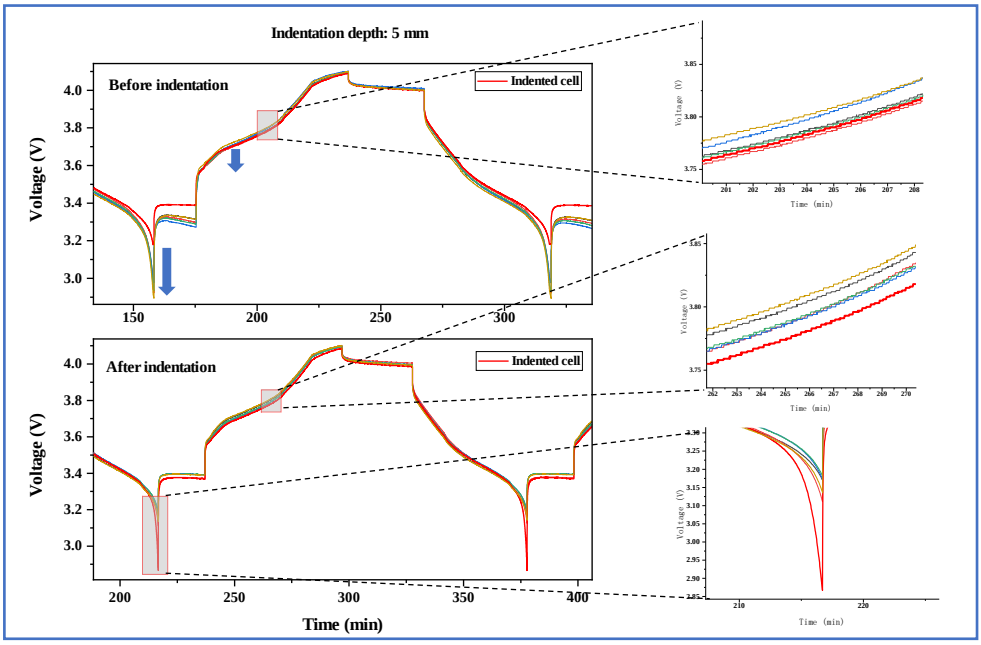

(**a**)

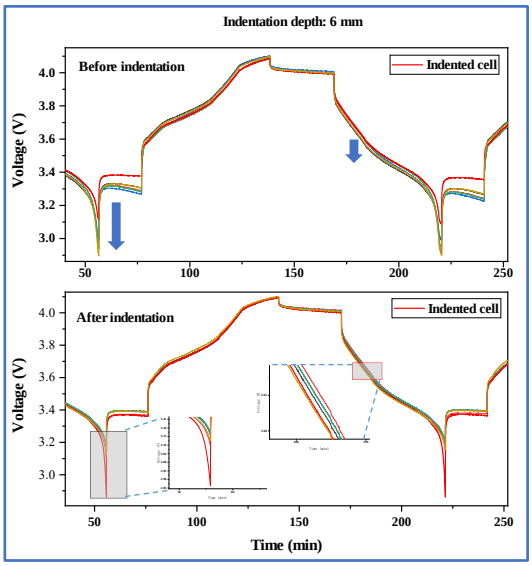

(**b**)

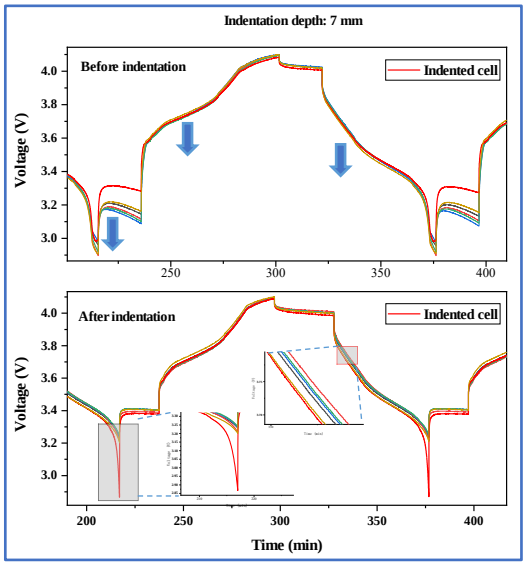

(**c**)

Figure 5. Voltage variation of battery module during charging and discharging periods at (**a**) 5 mm, (**b**) 6 mm, and (**c**) 7 mm depths of indentation.

Though the indented cell exhibits voltage deviation at the end of the discharge period, this feature may be difficult to identify and use for early warning due to the minor variation feature being easily disturbed by other factors such as the inherent inconsistency of the battery module itself. To better extract characteristic signals, the above voltage curves are transformed into *MN* values using Equation (1). Figure 6 presents the enlarged *MN* value of the cells' voltage in the charge−discharge cycle test of the battery module before and after indentation. These figures quantitatively describe the voltage deviation of each cell. Figure 6a shows that the *MN* values of the cells' voltage are distributed around 0 with a range of 0.01 in the charging and resting periods before the indentation. However, the *MN* value of the specified cell gradually deviates from the other cells and increases to 0.06 in the discharging period. At the same time, the *MN* value of the other cells declines below 0 due to the deviation of the specified cell elevating the average voltage $\overline{U}$. Figure 6b shows that the *MN* value of the indented cell's voltage remains below 0 and reaches a minimum in the charging period after indentation. At the end of discharge, the value sharply declines to −0.06. Meanwhile, the *MN* value of the other cells increases briefly. Accordingly, the voltage deviation of the indented cells shown in Figure 5a changes from higher to lower. The same feature of the *MN* value of the indented cells can also be observed in Figure 6c−f, where it is close to 0 at the beginning of charging and then declines to the lowest value at the end of discharging during the cycle test after indentation.

Figure 7 presents the *MN* value of the battery module during cycling after loading the mechanical abuse. Clearly, there is a sharp decline in the *MN* value of the indented cell and an increase in the *MN* value of other normal cells at the end of every discharging period. The minimum *MN* values of the indented cells under different mechanical loading conditions are compared in Figure 8. It can be observed that the minimum *MN* value decreases with an increase in indentation depth and cycle number, indicating that the voltage deviation of the indented cell gradually enlarges with an increase in cycle number and mechanical loading. The absolute values of these maximum *MN* values are beyond 0.04, which is much higher than that of normal cells. If the *MN* value is used for pre-warning, the indented cells can be easily detected by the sharp decline feature at the end of discharge using a threshold of −0.04.

To further explain the fault features that occur in mechanically abused cells, the capacities of indented cells were tested before and after mechanical loading through a cycle test. Figure 9a shows that the maximum capacity difference of indented cells with a 5 mm depth of indentation is 56 mAh. As shown in Figure 9b,c, the maximum capacity difference increases to 115 mAh and 163 mAh when the indentation depth increases to 6 mm and 7 mm, respectively. The average capacity degradation of indented cells at indentation depths of 5 mm, 6 mm, and 7 mm is 20 mAh, 83 mAh, and 140 mAh, respectively. It can be observed that the capacity degradation of the indented cell is similar to the capacity decline of the battery module shown in Figure 4, indicating that the capacity degradation of the indented cell leads to a decline in the battery module's capacity. The voltage inconsistency feature, including the lowest voltage distribution and the sharp voltage decline and corresponding *MN* value at the end of the discharging period as shown in Figure 6, is likely caused by the capacity degradation of indented cells combined with various internal resistances. According to a resistance analysis conducted in a previous study [32], the ohmic resistance is almost unchanged after the indentation, and the polarization resistance decreases slightly. Therefore, the voltage inconsistency feature at the end of discharging should be described by the variation in capacity. During the discharging period, the indented cell with a lower capacity than normal cells is more likely to reach the cut-off voltage.

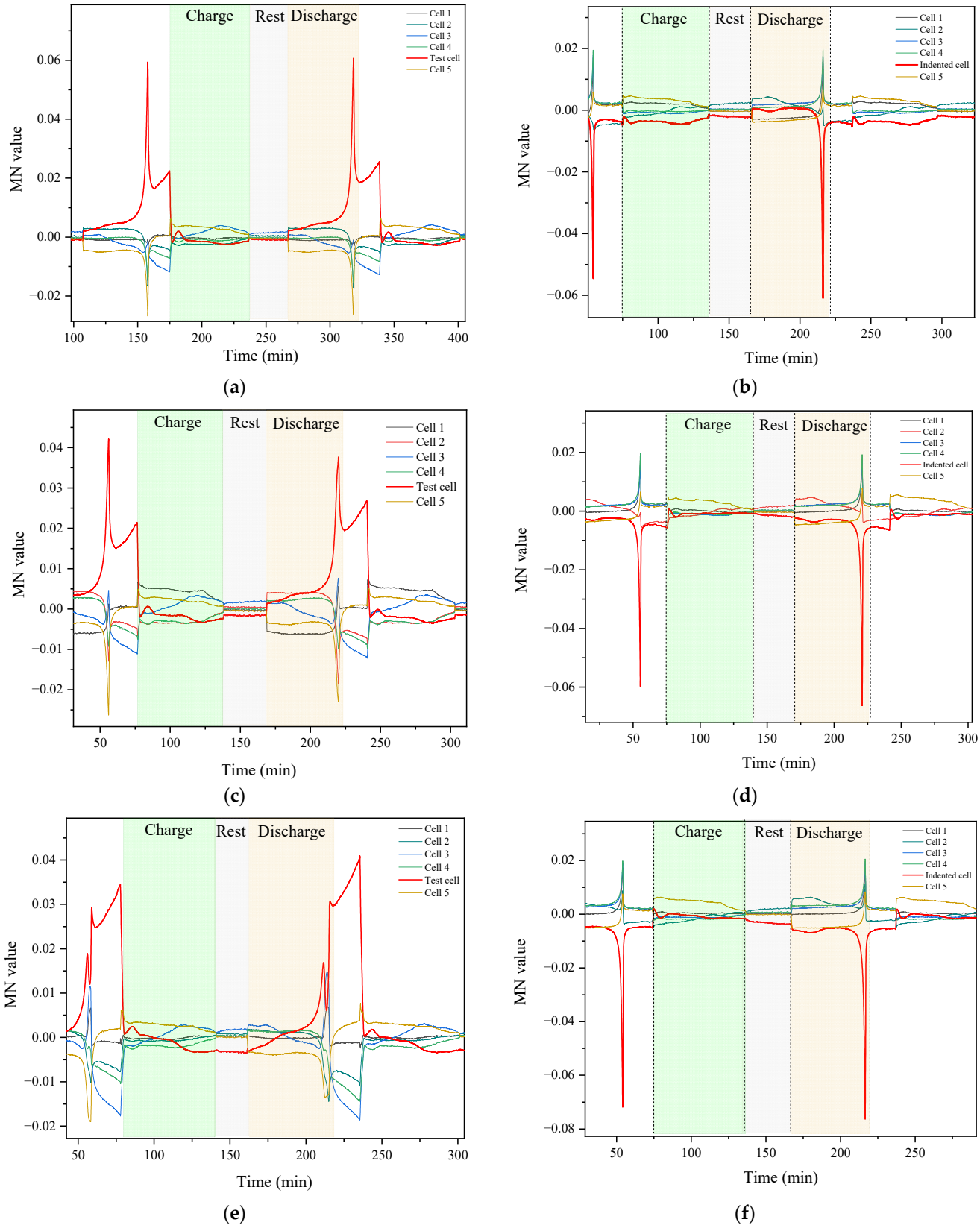

Figure 6. *MN* value of the battery voltage curves during charging and discharging cycle tests before and after the indentation test. (**a**) Before, (**b**) after 5 mm displacement of indentation; (**c**) before, (**d**) after 6 mm displacement of indentation; (**e**) before, (**f**) after 7 mm displacement of indentation.

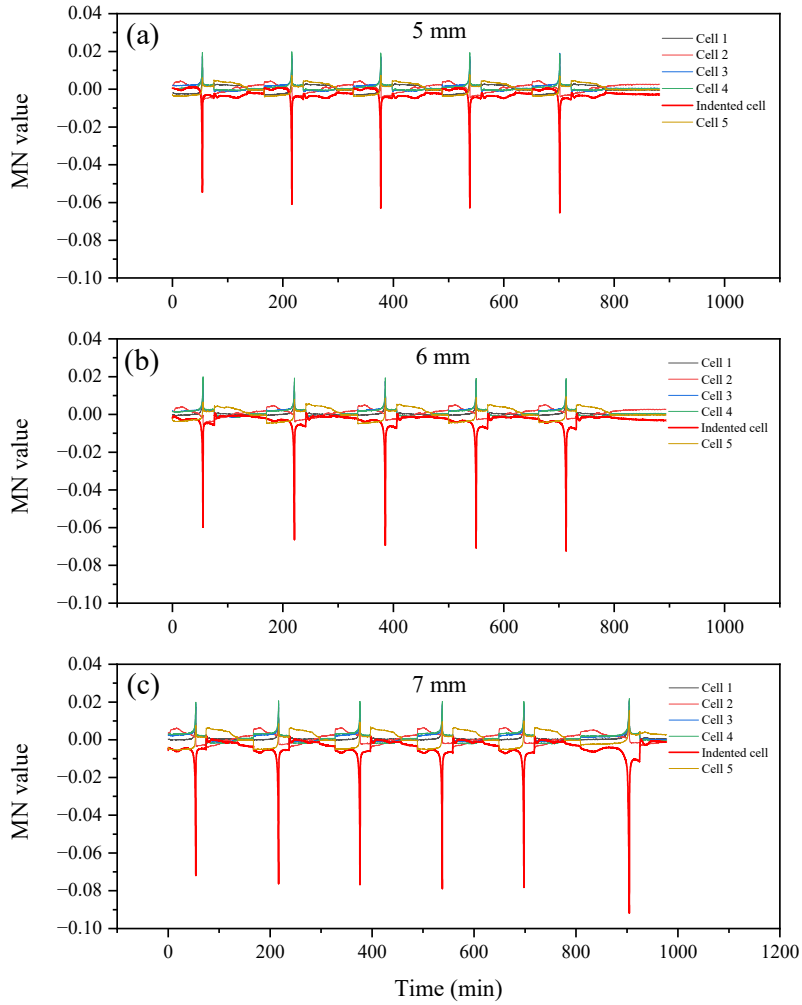

Figure 7. *MN* value of cells' voltage during cycling after loading (**a**) 5 mm, (**b**) 6 mm, (**c**) 7 mm depth of indentation.

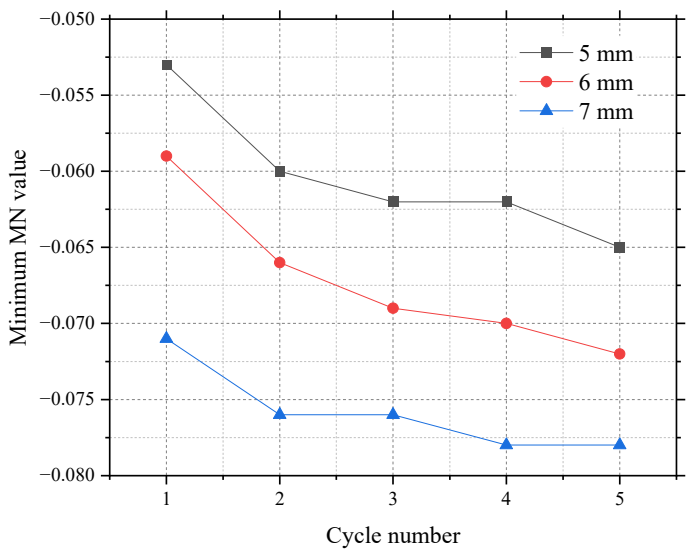

Figure 8. Minimum *MN* value of the indented cells during cycling after the indentation tests.

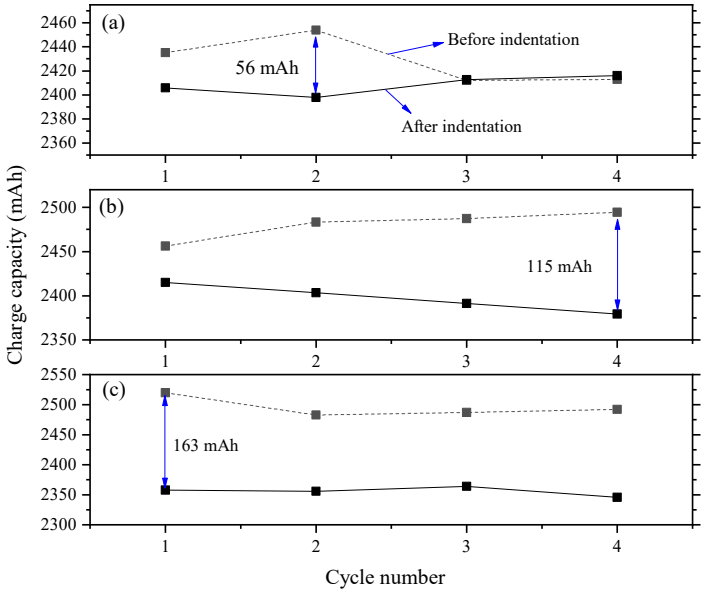

Figure 9. Capacity change of indented cells before and after the mechanical loading at (**a**) 5 mm, (**b**) 6 mm, and (**c**) 7 mm depths of indentation.

5. Conclusions

To detect and pre-warn against the mechanical deformation of abused cells, the variation in charge–discharge capacity and voltage consistency of the battery module under different degrees of mechanical deformation loading was analyzed. With an increase in indentation depth from 5 mm to 7 mm, the capacity of the battery module, with five normal cells and one indented cell connected in series, decreases by 132 mAh and 143 mAh in the charging and discharging periods, respectively. The voltage of the indented cell consistently shows the lowest voltage distribution during the charging and discharging periods. At the end of discharging, the voltage sharply declines and deviates significantly from the other normal cells. The *MN* value was employed to quantitatively analyze the voltage inconsistency, and the results indicate that the *MN* value can effectively describe the features of voltage inconsistency of cells. After mechanical deformation loading, the *MN* value of the voltage of the indented cell distributes at the lowest value during the charging period. At the end of discharging, the value sharply declines below -0.06, while the *MN* value of other normal cells briefly increases. The minimum *MN* value of indented cells during the cycling test decreases with an increase in indentation depth and cycle number, always staying below -0.04. This makes it suitable for the pre-warning of mechanical deformation using the *MN* method. The main reason for these features is due to capacity degradation after the cell undergoes mechanical deformation loading. In the future, a detailed theoretical framework and more experimental tests need to be conducted to reinforce the validity of the results. An online detection method for mechanical abuse will be established based on the features proposed in this study.

Author Contributions: Methodology, A.Z.; Software, H.Y.; Formal analysis, Y.Z. and H.Y.; Investigation, Y.Z., C.W. and S.L.; Resources, P.H.; Data curation, Y.Z., C.W. and S.L.; Writing—original draft, A.Z.; Writing—review and editing, P.H.; Supervision, P.H.; Project administration, C.W. and Z.B.; Funding acquisition, Z.B. All authors have read and agreed to the published version of the manuscript.

Funding: This research was funded by the Natural Science Foundation of Hunan province (No. 2020JJ4184) and the Fundamental Research Funds for the Central Universities (No. 531118010324).

Institutional Review Board Statement: Not applicable.

Informed Consent Statement: Informed consent was obtained from all subjects involved in the study.

Data Availability Statement: Data are contained within the article.

Conflicts of Interest: The authors declare that they have no known competing financial interests or personal relationships that could have appeared to influence the work reported in this paper.

Nomenclature

EV	electric vehicles
LIB	lithium-ion batteries
ISC	internal short circuit
SOC	state of charge
MN	Mean Normalization
BMS	battery management system
C-rate	charge rate
$\overline{U}$	mean value of the cells' voltage
U_{max}	maximum cell voltage
t_i	a specific moment in the voltage curve
k	the number of cells

References

1. Wang, Q.; Mao, B.; Stoliarov, S.I.; Sun, J. A review of lithium ion battery failure mechanisms and fire prevention strategies. *Prog. Energy Combust.* **2019**, *73*, 95–131. [CrossRef]
2. Song, L.; Zheng, Y.; Xiao, Z.; Wang, C.; Long, T. Review on Thermal Runaway of Lithium-Ion Batteries for Electric Vehicles. *J. Electron. Mater.* **2022**, *51*, 30–46. [CrossRef]
3. Feng, X.; Ren, D.; He, X.; Ouyang, M. Mitigating Thermal Runaway of Lithium-Ion Batteries. *Joule* **2020**, *4*, 743–770. [CrossRef]
4. Hu, G.; Huang, P.; Bai, Z.; Wang, Q.; Qi, K. Comprehensively analysis the failure evolution and safety evaluation of automotive lithium ion battery. *eTransportation* **2021**, *10*, 100140. [CrossRef]
5. Liu, B.; Jia, Y.; Yuan, C.; Wang, L.; Gao, X.; Yin, S.; Xu, J. Safety issues and mechanisms of lithium-ion battery cell upon mechanical abusive loading: A review. *Energy Storage Mater.* **2020**, *24*, 85–112. [CrossRef]
6. Zeng, G.; Bai, Z.; Huang, P.; Wang, Q. Thermal safety study of Li-ion batteries under limited overcharge abuse based on coupled electrochemical-thermal model. *Int. J. Energ. Res.* **2020**, *44*, 3607–3625. [CrossRef]
7. Xiong, R.; Yang, R.; Chen, Z.; Shen, W.; Sun, F. Online Fault Diagnosis of External Short Circuit for Lithium-Ion Battery Pack. *IEEE Trans. Ind. Electron.* **2020**, *67*, 1081–1091. [CrossRef]
8. Zhang, X.; Chen, S.; Zhu, J.; Gao, Y. A Critical Review of Thermal Runaway Prediction and Early-Warning Methods for Lithium-Ion Batteries. *Energy Mater. Adv.* **2023**, *4*, 8. [CrossRef]
9. Tran, M.; Mevawalla, A.; Aziz, A.; Panchal, S.; Xie, Y.; Fowler, M. A Review of Lithium-Ion Battery Thermal Runaway Modeling and Diagnosis Approaches. *Processes* **2022**, *10*, 1192. [CrossRef]
10. Hu, X.; Zhang, K.; Liu, K.; Lin, X.; Dey, S.; Onori, S. Advanced Fault Diagnosis for Lithium-Ion Battery Systems: A Review of Fault Mechanisms, Fault Features, and Diagnosis Procedures. *IEEE Ind. Electron. Mag.* **2020**, *14*, 65–91. [CrossRef]
11. Zhu, X.; Wang, Z.; Wang, Y.; Wang, H.; Wang, C.; Tong, L.; Yi, M. Overcharge investigation of large format lithium-ion pouch cells with $Li(Ni_{0.6}Co_{0.2}Mn_{0.2})O_2$ cathode for electric vehicles: Thermal runaway features and safety management method. *Energy* **2019**, *169*, 868–880. [CrossRef]
12. Yao, L.; Wang, Z.; Ma, J. Fault detection of the connection of lithium-ion power batteries based on entropy for electric vehicles. *J. Power Sources* **2015**, *293*, 548–561. [CrossRef]
13. Wang, Z.P.; Hong, J.C.; Liu, P.; Zhang, L. Voltage fault diagnosis and prognosis of battery systems based on entropy and Z-score for electric vehicles. *Appl. Energ.* **2017**, *196*, 289–302. [CrossRef]
14. Mao, B.; Chen, H.; Cui, Z.; Wu, T.; Wang, Q. Failure mechanism of the lithium ion battery during nail penetration. *Int. J. Heat. Mass. Tran.* **2018**, *122*, 1103–1115. [CrossRef]
15. Ramadass, P.; Fang, W.; Zhang, Z.J. Study of internal short in a Li-ion cell I. Test method development using infra-red imaging technique. *J. Power Sources* **2014**, *248*, 769–776. [CrossRef]
16. Qiao, D.; Wang, X.; Lai, X.; Zheng, Y.; Wei, X.; Dai, H. Online quantitative diagnosis of internal short circuit for lithium-ion batteries using incremental capacity method. *Energy* **2022**, *243*, 123082. [CrossRef]
17. Samsung Electronics Announces the Reasons for the Combustion of the Note7 with a Third Party. Available online: https://www.bbc.com/news/business-38714461 (accessed on 23 January 2017).
18. Samsung Confirms Battery Faults as Cause of Note 7 Fires. Available online: https://www.icauto.com.cn/vvauto/66/661391.html (accessed on 10 September 2021).
19. Sahraei, E.; Hill, R.; Wierzbicki, T. Calibration and finite element simulation of pouch lithium-ion batteries for mechanical integrity. *J. Power Sources* **2012**, *201*, 307–321. [CrossRef]
20. Duan, X.; Wang, H.; Jia, Y.; Wang, L.; Liu, B.; Xu, J. A multiphysics understanding of internal short circuit mechanisms in lithium-ion batteries upon mechanical stress abuse. *Energy Storage Mater.* **2022**, *45*, 667–679. [CrossRef]

21. Li, W.; Xia, Y.; Chen, G.; Sahraei, E. Comparative study of mechanical-electrical-thermal responses of pouch, cylindrical, and prismatic lithium-ion cells under mechanical abuse. *Sci. China Technol. Sci.* **2018**, *61*, 1472–1482. [CrossRef]
22. Zhu, J.; Zhang, X.; Sahraei, E.; Wierzbicki, T. Deformation and failure mechanisms of 18650 battery cells under axial compression. *J. Power Sources* **2016**, *336*, 332–340. [CrossRef]
23. Wang, H.; Simunovic, S.; Maleki, H.; Howard, J.N.; Hallmark, J.A. Internal configuration of prismatic lithium-ion cells at the onset of mechanically induced short circuit. *J. Power Sources* **2016**, *306*, 424–430. [CrossRef]
24. Santhanagopalan, S.; Ramadass, P.; Zhang, J.Z. Analysis of internal short-circuit in a lithium ion cell. *J. Power Sources* **2009**, *194*, 550–557. [CrossRef]
25. Xu, J.; Liu, B.; Hu, D. State of Charge Dependent Mechanical Integrity Behavior of 18650 Lithium-ion Batteries. *Sci. Rep.* **2016**, *6*, 21829. [CrossRef]
26. Huang, L.; Liu, L.; Lu, L.; Feng, X.; Han, X.; Li, W.; Zhang, M.; Li, D.; Liu, X.; Sauer, D.U.; et al. A review of the internal short circuit mechanism in lithium-ion batteries: Inducement, detection and prevention. *Int. J. Energ. Res.* **2021**, *45*, 15797–15831. [CrossRef]
27. Zhu, X.; Wang, H.; Allu, S.; Gao, Y.; Cakmak, E.; Hopkins, E.J.; Veith, G.M.; Wang, Z. Investigation on capacity loss mechanisms of lithium-ion pouch cells under mechanical indentation conditions. *J. Power Sources* **2020**, *465*, 228314. [CrossRef]
28. Li, L.; Chen, X.; Hu, R.; Wang, T.; Ji, H.; Yuan, Q.; Ji, Y.; Jiang, Z.; Liu, W.; Zheng, W. Aging Mechanisms and Thermal Characteristics of Commercial 18650 Lithium-Ion Battery Induced by Minor Mechanical Deformation. *J. Electrochem. Energy* **2021**, *18*, 21010. [CrossRef]
29. Cannarella, J.; Arnold, C.B. Stress evolution and capacity fade in constrained lithium-ion pouch cells. *J. Power Sources* **2014**, *245*, 745–751. [CrossRef]
30. Wang, H.; Leonard, D.N.; Meyer, H.M.; Watkins, T.R.; Kalnaus, S.; Simunovic, S.; Allu, S.; Turner, J.A. Microscopic analysis of copper current collectors and mechanisms of fragmentation under compressive forces. *Mater. Today Energy* **2020**, *17*, 100479. [CrossRef]
31. Sahraei, E.; Gilaki, M.; Lynch, W.; Kirtley, J.; Soudbakhsh, D. Cycling Results of Mechanically Damaged Li-Ion Batteries. In Proceedings of the 2019 IEEE Electric Ship Technologies Symposium (ESTS), Washington, DC, USA, 14–16 August 2019; IEEE: Piscateville, NJ, USA, 2019; pp. 226–230.
32. Huang, P.F.; Liu, S.T.; Ma, J.; Zheng, G.; Li, E.; Wei, M.Y.; Wang, Q.S.; Bai, Z.H. Comprehensive investigation on the durability and safety performances of lithium-ion batteries under slight mechanical deformation. *J. Energy Storage* **2023**, *66*, 107450. [CrossRef]
33. Liu, Y.; Xia, Y.; Zhou, Q. Effect of low-temperature aging on the safety performance of lithium-ion pouch cells under mechanical abuse condition: A comprehensive experimental investigation. *Energy Storage Mater.* **2021**, *40*, 268–281. [CrossRef]
34. Xing, B.; Xiao, F.; Korogi, Y.; Ishimaru, T.; Xia, Y. Direction-dependent mechanical-electrical-thermal responses of large-format prismatic Li-ion battery under mechanical abuse. *J. Energy Storage* **2021**, *43*, 103270. [CrossRef]